Inorganic Chemistry

Article

pubs.acs.org/IC

In Situ Energy-Dispersive X-ray Diffraction for the Synthesis Optimization and Scale-up of the Porous Zirconium Terephthalate UiO-66

Florence Ragon,[†,∥] Patricia Horcajada,*[,†] Hubert Chevreau,[†,⊥] Young Kyu Hwang,[‡] U-Hwang Lee,[‡] Stuart R. Miller,[†,⊗] Thomas Devic,[†] Jong-San Chang,[‡,§] and Christian Serre*[,†]

[†]Institut Lavoisier, UMR CNRS 8180, Université de Versailles Saint-Quentin-en-Yvelines, 45 avenue des États-Unis, 78035 Versailles cedex, France

[‡]Research Group for Nanocatalyst, Biorefinery Research Center, Korea Research Institute of Chemical Technology (KRICT), P.O. Box 107, Daejeon, Yusung 305-600, Republic of Korea

[§]Department of Chemistry, Sungkyunkwan University, Suwon 440-476, Republic of Korea

Supporting Information

ABSTRACT: The synthesis optimization and scale-up of the benchmarked microporous zirconium terephthalate UiO-66(Zr) were investigated by evaluating the impact of several parameters (zirconium precursors, acidic conditions, addition of water, and temperature) over the kinetics of crystallization by time-resolved in situ energy-dispersive X-ray diffraction. Both the addition of hydrochloric acid and water were found to speed up the reaction. The use of the less acidic $ZrOCl_2 \cdot 8H_2O$ as the precursor seemed to be a suitable alternative to $ZrCl_4 \cdot xH_2O$, avoiding possible reproducibility issues as a consequence of the high hygroscopic character of $ZrCl_4$. $ZrOCl_2 \cdot 8H_2O$ allowed the formation of smaller good quality UiO-66(Zr) submicronic particles, paving the way for their use within the nanotechnology domain, in addition to higher reaction yields, which makes this synthesis route suitable for the preparation of UiO-66(Zr) at a larger scale. In a final step, UiO-66(Zr) was prepared using conventional reflux conditions at the 0.5 kg scale, leading to a rather high space-time yield of 490 kg m^{-3} day^{-1}, while keeping physicochemical properties similar to those obtained from smaller scale solvothermally prepared batches.

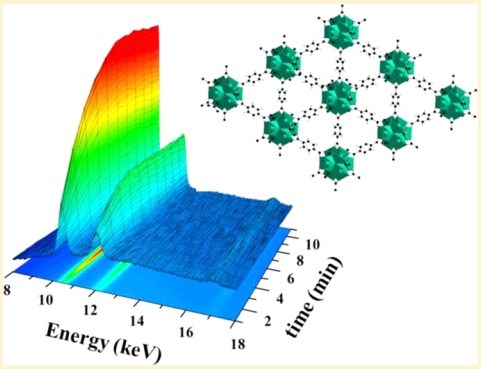

INTRODUCTION

Metal−organic frameworks (MOFs)[1] have recently generated great interest due to their high degree of porosity and easily tunable structure and composition, which offer various opportunities[2,3] in societal-relevant fields of applications such as gas separation or storage,[4−7] catalysis,[8,9] or biomedicine,[10,11] among others. Although these applications are still at an exploratory level, Czaja et al.[12] have noticed that gas storage, purification, and separation are very promising and are expected to lead to industrial developments within the next decade. Indeed, aluminum-based MOFs are currently developed for natural gas storage in heavy-duty vehicles.[13,14] Additionally, the number of patents concerning MOF applications has significantly increased in recent years, evidencing the great interest to the industry.[15−24] Consequently, the development of well-adapted, scalable, safe, and cheap synthetic methods of MOFs is a prerequisite for further industrial expansion. The chemical company BASF has been working over the past two decades toward larger-scale synthesis of MOFs, developing alternatives to static hydro- or solvothermal preparation methods, such as (i) the round-bottom flask route (using a conventional reflux setup) validated with the zinc terephthalates MOF-2 and MOF-5 and the zinc 2,6-naphthalene dicarboxylate IRMOF-8[25] and (ii) the electrochemical route using the copper trimesate Cu-EMOF (also known as HKUST-1) and the zinc 2-methylimidazolate Zn-EZIF (also called ZIF-8).[15,16,25] It is worth noting that conventional reflux setup conditions have been stated as being reproducible at the kg scale, using a 159 L reactor.[25] Furthermore, five MOFs are currently marketed through Sigma-Aldrich:[26] an aluminum terephthalate MIL-53(Al),[24] HKUST-1,[15] an iron trimesate (FeBTC), a zinc 2-methyl imidazolate ZIF-8,[16] and a magnesium formate,[22] respectively named Basolite A100, Basolite C300, Basolite F300, Basolite Z1200, and Basosiv M050.[12] For scale-up production, space-time yield (STY) is a parameter of prime importance, as it represents the mass of MOF formed per volume of the reactor and time (kg m^{-3} s^{-1}).[27] Notably, the water-based synthesis at ambient pressure of a porous aluminum fumarate called Basolite A520 has been reported with an unprecedented STY of 5600 kg m^{-3} day^{-1},[13,14,23] while the Korean Research Institute of Chemical Engineering

Received: October 4, 2013
Published: February 14, 2014

   dx.doi.org/10.1021/ic402514n | Inorg. Chem. 2014, 53, 2491−2500

(KRICT) has developed both the HF-free synthesis of the mesoporous iron trimesate MIL-100(Fe), using a 10 L autoclave, with a very high STY of 1300 kg m^{-3} day^{-1},[20,28] as well as the continuous microwave-assisted synthesis of HKUST-1 with a STY of 2000 kg m^{-3} day^{-1}.[17,21,29] More recently, Cbana Laboratories Inc.[30] have also proposed the large-scale preparation of MOFs such as the Banasorb 22, Banasorb 24, and Banasorb 30, all presenting a similar topology to the MOF-5 solid but with different hydrophobic functional groups on the aromatic ring of the terephthalate linker (respectively trifluoromethoxy, dimethyl, and methyl group) to improve the moisture stability of the water-unstable MOF-5.[31]

Another obstacle that can limit the industrial use of some MOFs is their sometimes low thermal, hydrothermal, and chemical stabilities in comparison with commercialized porous materials such as zeolites. Indeed, working conditions often involve high temperatures for vapor or gas-phase processes or acidic or basic conditions for liquid-phase reactions, requiring therefore highly stable materials. Low et al.[32] have assessed the hydrostability of MOFs by building a "steam stability map," showing that for a given linker, the moisture stability of the MOF increases as a function of the charge of the metal cation. Thus, tetravalent metals (i.e., zirconium, titanium) might lead to highly stable MOFs. This is the case of the zirconium(IV) terephthalate UiO-66(Zr)[33] (UiO for University of Oslo), a three-dimensional cubic close packed (CCP) structure built up from $Zr_6(O)_4(OH)_4$ oxoclusters linked together by 12 terephthalate linkers (Supporting Information, Figure S1a). The UiO-66(Zr) solid exhibits tetrahedral and octahedral cages of 6 and 11 Å, respectively, accessible through microporous windows (4−6 Å) (Supporting Information, Figure S1b,c), leading to a high porosity (BET surface area ≈ 1200 m^2 g^{-1}, pore volume ≈ 0.47 cm^3 g^{-1}) combined with a high thermal (up to 723 K under air), chemical (hydrothermal, organic solvents, acidic conditions), and mechanical stability (up to 10 000 kg cm^{-2}).[33−35] Furthermore, textural and physicochemical properties of the UiO-66(Zr) solid can be easily tuned by using functionalized terephthalate linkers (NH_2, Br, NO_2, etc.) or extended organic ligands (e.g., naphthalene, biphenyl, terphenyl, or azobenzenedicarboxylates).[36−38] Because of these interesting properties, the UiO-66(Zr) solid appears to be a good candidate in adsorption,[34,39−41] separation,[42] photochemical,[43] catalysis,[44,45] and drug carrier applications.[46] Accordingly, developing low-cost UiO-66(Zr) synthesis processes compatible with an industrial scale-up is of great importance.

Up to now, the UiO-66(Zr) solid has been exclusively synthesized under solvothermal conditions, using zirconium tetrachloride ($ZrCl_4$) as a Zr source. The UiO-66(Zr) solid was first prepared by Cavka et al.[33] under diluted solvothermal conditions using a mixture of commercially available terephthalic acid (H_2BDC) and $ZrCl_4$ in *N*,*N*-dimethylformamide (DMF) at 393 K for 24 h. Alternative synthetic conditions mainly based on the modulation approach by using different additives were later proposed to control both the size and the morphology of the UiO-66(Zr) crystallites. Abid et al.[47] observed that the addition of ammonium hydroxide (NH_4OH) leads to the formation of smaller crystal size (ranging from 63.2 to 17.1 nm). Behrens et al.[48,49] highlighted the influence of several modulators such as formic, benzoic, acetic, and hydrochloric acids (HCl) on the synthesis of different zirconium dicarboxylate MOFs with the UiO-66(Zr) solid topology, noticing for instance (i) a better crystallinity and reproducibility when benzoic or acetic acid was used,[48] (ii) that some UiO-66(Zr)-type materials, such as the Zr-fumarate, were only obtained in the presence of formic acid,[49] and (iii) the absence of an effect from the addition of HCl on the zirconium 4,4′-biphenyldicarboxylate UiO-67(Zr)[33] synthesis.[48] Some of us have however noticed an improvement of the crystallinity of its isostructural analogue zirconium terephthalate UiO-66(Zr) when small amounts of HCl were added.[34,41,42,50] Additionally, Katz et al.[51] have evidenced an acceleration of the UiO-66(Zr)-type MOFs formation when HCl was added. Finally, Vermoortele et al.[45] have recently also used the modulation approach to increase the catalytic activity of the UiO-66(Zr). The combined used of HCl and trifluoroacetic acid in the synthesis has resulted in a highly crystalline material with partial substitution of terephthalates by trifluoroacetates.

Several groups have lately focused their attention of late on the large-scale preparation of UiO-66(Zr) solid, with the aim of evaluating its performance in different strategic applications. Serre et al.[34,41,42,50] reported a static solvothermal scale-up synthesis in DMF with ca. 66% yield (STY of 29 kg m^3 day^{-1}). Similarly, Lillerud et al.[37] described the static DMF synthesis of three functionalized UiO-66(Zr) solids (Br, NH_2, and NO_2) and Vermoortele et al.[44] adapted these solvothermal conditions to prepare at the multigram scale the amino version of the UiO-66(Zr) solid in DMF in the presence of water. However, the yields of these later examples were not reported. More recently, Katz et al.[51] have reported a large-scale synthesis of UiO-66(Zr), yielding 7.2 g of the preactivated compound, and Schoenecker et al.[52] have both developed a continuous-flow synthesis and scaled up the preparation of UiO-66(Zr)-NH_2 from a 5 to 250 mL sealed borosilicate glass without however any improvement to the yield (STY of 9 kg m^3 day^{-1}). Nevertheless, the solvothermal route is difficult to extend to industrially compatible larger-scale conditions due to safety, cost, and reproducibility issues. The concomitant use of ambient pressure, an easy and homogeneous stirring, relatively cheap and easily adaptable components of the round bottom flask setup presented here represents a key advantage over the previous solvothermal synthesis route. The scale-up of a given solid also requires an understanding of its crystallization through the investigation of the effect of the experimental parameters. Schoenecker et al.[52] reported the ex situ investigation of the crystallization of UiO-66(Zr)-NH_2 solid and deduced that nucleation and growth take place at the same time during the reaction. Although ex situ studies are easy to conduct under laboratory conditions, they sometimes lead to nonreliable results due to a possible change in the nature of the quenched sample or due to unsatisfactory control of the heating rate. The in situ energy-dispersive X-ray diffraction (EDXRD) technique is a suitable approach to analyze the crystallization of porous solids. So far, this tool has been applied to the crystallization study of different MOFs such as MIL-53(Fe),[53] HKUST-1,[53,54] MOF-14,[54] CAU-1(Al)-$(OH)_2$,[55] CAU-1(Al)-NH_2,[56] ZIF-8,[57] a lithium carboxylate,[58] MIL-100(Mn),[59] and CPO-27(Co, Ni).[60]

To the best of our knowledge, no such study has been reported to date for UiO-66(Zr). We report here the use of time-resolved in situ diffraction experiments (EDXRD) with the aim to optimize and scale up the synthesis of this promising porous material. Here, the nature of the zirconium precursor, acidic conditions, cosolvent, time, and temperature were evaluated and led to the estimation of the rate of crystallization

dx.doi.org/10.1021/ic402514n | Inorg. Chem. 2014, 53, 2491−2500

and the activation energy. On the basis of these results, an optimized, ambient pressure synthesis route for the large-scale preparation (0.5 kg) of the UiO-66(Zr) solid is finally proposed.

EXPERIMENTAL SECTION

Materials. All chemicals were obtained commercially and used without further purification.

In Situ Crystallization Studies. UiO-66(Zr) solid was solvothermally obtained from an equimolar DMF solution (Carlo Erba, pure) of 1,4-benzenedicarboxylic acid (H_2BDC) (Aldrich, 98%) and either $ZrOCl_2{\cdot}8H_2O$ (Alfa Aesar, 98%) or $ZrCl_4$ (Alfa Aesar, 99.5 +%) in the temperature range of 343−423 K. A reaction volume of around 2 mL and a 0.2 M zirconium concentration were kept constant. The influence of different parameters such as metal precursor, water cosolvent, acidic conditions, and temperature was studied through the evaluation of the kinetics, crystallinity, and yields (see Supporting Information, Tables S1 and S2). The synthesis was performed in borosilicate Schott DURAN culture tubes of 8 mL total volume and heated using a conventional oven for which temperature was electronically controlled to ±2 K (see Engelke et al.[61] for details). The tubes were sealed by a screw cap. Reaction mixtures were rapidly stirred during data collection to ensure that solid material remains in the X-ray beam during all the measurement.

Lab-Scale Synthesis (1 L Reactor). UiO-66(Zr) was synthesized in a 1 L round-bottom flask, equipped with a reflux condenser and a mechanical Teflon-lined stirrer. H_2BDC (16.6 g, 0.1 mol) (Aldrich, 98%) was dissolved in 500 mL of DMF (474 g, 6.5 mol) at room temperature under stirring. $ZrOCl_2{\cdot}8H_2O$ (32.2 g, 0.1 mol) (Alfa Aesar, 98%) and 6 mL of 37% HCl (7 g, 0.2 mol) were added to the mixture. The molar ratio of the final $ZrOCl_2{\cdot}8H_2O/H_2BDC/DMF/HCl$ mixture is 1:1:65:2. The mixture was heated at reflux ($T \approx 423$ K) under stirring for 24 h. Mechanical rather than magnetic stirring was found to be of prime importance to avoid the complete solidification of the mixture. The obtained white gel-consistency solid was recovered by filtration, washed with DMF at room temperature, and dried at 373 K overnight. The activation was performed in three steps. To remove the free H_2BDC, 1 g of solid was first dispersed in 100 mL of DMF at room temperature under stirring overnight. The same procedure was repeated twice, using methanol (MeOH) instead of DMF to exchange the DMF. Finally, the solid was dried at 373 K overnight to remove MeOH and left under air in atmospheric condition. Yield based on zirconium: 80%.

Lab-Scale Synthesis (5 L Reactor). The scale-up synthesis using a high concentration of $ZrOCl_2{\cdot}8H_2O$ was carried out in a 5 L glass reactor (Reactor Master, Syrris) equipped with a reflux condenser and a Teflon-lined mechanical stirrer having two blades. For a typical synthesis, 462 g (2.8 mol) of H_2BDC (98%) were initially dissolved in 2.5 L of DMF (2.36 kg, 32.3 mol) at room temperature. Then, 896 g (2.8 mol) of $ZrOCl_2{\cdot}8H_2O$ (98%) and 465 mL of 37% HCl (548 g, 15 mol) were added to the mixture. The molar ratio of the final $ZrOCl_2{\cdot}8H_2O/H_2BDC/DMF/HCl$ mixture is 1:1:11.6:5.4. The reaction mixture was vigorously stirred, leading to a homogeneous gel. The mixture was then heated to 423 K with a ramping rate of 1 K min^{-1} and kept at this temperature for 6 h in the reactor without stirring, leading to crystalline UiO-66(Zr) solid. The resulting product (∼510 g) was recovered from the slurry by filtration, redispersed in 7 L of DMF at 333 K for 6 h under stirring, and recovered by filtration. The same procedure was repeated twice, using MeOH instead of DMF. The solid product was finally dried at 373 K overnight. Yield based on zirconium: 67%.

Characterization. Laboratory X-ray powder diffraction (XRPD) data were recorded using a conventional high-resolution ($\theta-2\theta$) Siemens D5000 diffractometer with Cu Kα radiation ($\lambda \approx 1.54056$ Å).

In Situ Energy-Dispersive X-ray Diffraction (EDXRD). Product formation was studied by in situ EDXRD on the Beamline F3 of the HASYLAB facility (DESY, Hamburg, Germany). This beamline receives white synchrotron radiation with energy of 13.5−65 keV, and the incident X-ray beam is collimated to 20 × 20 mm^2. Scattered X-rays were detected using a liquid-nitrogen-cooled solid-state germanium detector positioned at around 2.92° and data accumulated in 30, 60, or 120 s intervals. From collected EDXRD spectra, the extent of crystallization α was extracted by integration of the most intense Bragg peaks, namely, the (111) and (200) peaks for UiO-66(Zr) solid (see Supporting Information, Figure S1 and Table S3). Although the third peak (corresponding to (220) Bragg reflection) can be observed, its rather limited signal-to-noise ratio precludes an accurate integration. All integrated intensities were normalized by the zirconium fluorescence to take into account the drop of the beam as a function of time and scaled from zero at the beginning of the reaction to unity at the end. The integration of these Bragg peaks was performed using different tools: (i) "calf3" (software offered and available for free at beamline F3, private copy by A. Rothkirch/DESY) and (ii) "Peak Analyser" contained in the software Origin (OriginLab, Northampton, MA). Integration using both software programs was not significantly different (Supporting Information, Figure S2). The crystallization time t_f corresponds to the time when no increase of peak intensity is observed, characterized by the presence of a plateau on the crystallization curve. The induction period t_0 is the time required to detect any crystallinity (normalized peak intensity >5%).

Fourier transform infrared spectroscopy (FT-IR) spectra were recorded on a Nicolet 6700 FT-IR thermo scientific spectrometer in the 350−4000 cm^{-1} region.

Nitrogen adsorption was performed at 77 K, using commercially available equipment (BEL Japan, Belsorp Mini). Prior to the measurement, the sample was treated under primary vacuum at 473 K overnight (BEL Japan, BELSORP Prep). Specific surface areas were calculated according to the Langmuir and BET equations.

Thermogravimetric analysis (TGA) curves were performed on a STA6000 simultaneous thermal analyzer from Perkin-Elmer, under O_2 atmosphere (20 mL min^{-1}) between room temperature and 873 K, at a heating rate of 2 K min^{-1}.

Dynamic light scattering (DLS) measurements were performed on a Zetasizer Nano ZS from Malvern Instruments. The solid materials were dispersed in ethanol by ultrasound, with a Digital Sonifer probe (Branson Ultrasonics Corporation, 400 W) at 10% of amplitude for 30 s.

RESULTS AND DISCUSSION

Time-Resolved in Situ EDXRD Studies. For a better understanding of the role of HCl on the UiO-66(Zr) crystallization, the influence of acidic conditions was investigated at 423 K by adding different amounts of a concentrated (37%) aqueous solution of HCl (0 to 10 equiv per zirconium; see Supporting Information, Table S1), while keeping the total volume and concentration constant (2 mL and 0.2 M), that is, by replacing a fraction of DMF by the HCl solution. Considering the inevitable addition of water and the previous studies reported by Behrens et al.[48] showing that water plays a crucial role in the synthesis of Zr-based MOFs, similar experiments were conducted by adding the same amount of pure water as was present in the added HCl aqueous solution (see Supporting Information, Table S2). Crystallization was followed by in situ EDXRD; for instance, the crystallization process at 423 K with 1 equiv of H_2O/Zr is shown in Figure 1, while Figure 2 and Supporting Information, Figure S3 show the normalized crystallization curves produced by the integration of the (111) and (200) Bragg peaks (see Supporting Information, Figure S1d for the XRD pattern).

Importantly, only amorphous product was obtained using pure DMF without addition of HCl after 2 h of reaction, whereas a faster crystallization rate of the UiO-66(Zr) phase was observed upon the addition of HCl. To extract the kinetic information from the EDXRD data, crystallization curves were analyzed further, using the Avrami−Erofe'ev (AE)[62,63]

dx.doi.org/10.1021/ic402514n | Inorg. Chem. 2014, 53, 2491−2500

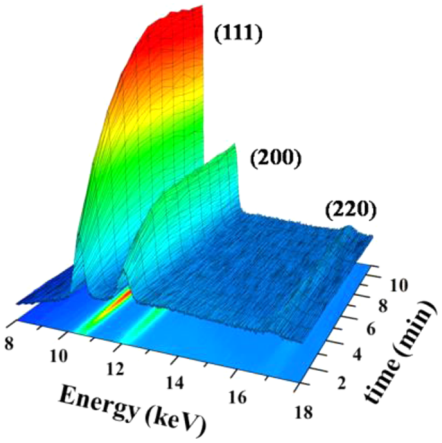

Figure 1. Time-resolved in situ EDXRD data of the solvothermal synthesis of UiO-66(Zr) solid synthesized at 423 K from $ZrCl_4$ precursor with 1 equiv of H_2O/Zr. The main reflections of UiO-66(Zr) solid are indexed in the figure.

equation, which relates the extent of crystallization α to the reaction time t and the induction time t_0 (eq 1). This equation was further linearized using Sharp and Hancock method (SH) (eq 2),[64] allowing the extraction of the Avrami exponent n_{SH} and the rate constant k_{SH} (Table 1 and Supporting Information, Table S4).

$$\alpha = 1 - \exp(-k_{SH}(t - t_0))^{n_{SH}} \quad (1)$$

$$\ln(-\ln(1 - \alpha)) = n_{SH} \ln k_{SH} + n_{SH} \ln(t - t_0) \quad (2)$$

Following the most intense (111) Bragg peak, the rate constant k_{SH} increases with the amount of HCl, leading to very fast formation rates at high HCl/Zr ratio (see inset plot in Figure 2a). Indeed, the time needed to reach the maximum crystallinity is only 6 and 5 min for HCl/Zr = 7.5 and 10 equiv, respectively. However, the lowest tested HCl concentration (HCl/Zr = 1 equiv) leads to slower kinetics (total crystallization time = 84 min). These results, together with the absence of noticeable crystallization in the absence of HCl, could, at first sight, appear counterintuitive. One would indeed expect that highly acidic conditions would favor the protonation of the linker and thus decrease the crystallization rate. Here, the faster crystallization rate might be related to the easier formation of the Zr^{4+}oxo/hydroxo clusters, which is favored in the presence of water in the HCl source, in agreement with the chemistry of zirconium in water, as shown on the corresponding Pourbaix diagram.[65] To verify this hypothesis, in a second set of experiments, pure water was added. As shown in Figure 2b and Table 1, for a given amount of water (x equiv of H_2O/Zr = amount of H_2O added upon addition of x equiv of HCl/Zr), crystallization without HCl is always faster than that with HCl. Thus, if water favors the formation of the oxoclusters, more acidic conditions lead to slower kinetics, probably due to the decrease in the deprotonation rate of the carboxylic linker. At lower amounts (HCl or H_2O/Zr = 1 equiv), the UiO-66(Zr) formation was around 10 times faster in presence of equivalent amounts of water than the aqueous solution of HCl (k_{SH} = 0.034 vs 0.396 min^{-1}). This difference becomes nevertheless less significant for higher concentrations (k_{SH} = 0.894 vs 1.203 min^{-1} for 10 equiv of HCl and H_2O, respectively). It could be also speculated that once a certain amount of water is added, the crystallization of the solid no longer depends on the amount of water, explaining the small difference observed at high HCl and H_2O contents. Similar tendencies were also noted concerning the data fitting from the (200) Bragg peak (Supporting Information, Figure S3 and Table S4).

Furthermore, the value of the Avrami exponent coefficient n_{SH} might provide some information concerning the crystallization mechanism.[66] Here, in all cases, the low value of n_{SH}

Table 1. [a]

additive (equiv/Zr)	t_f (min)	t_0 (min)	n_{SH}	k_{SH} (min^{-1})
1 HCl	84	6	1.00	0.03
3 HCl	20	4	0.78	0.14
5 HCl	14	2	1.06	0.26
7.5 HCl	6	1	1.94	0.49
10 HCl	5	1	1.50	0.89
1 H_2O	5	0	1.41	0.40
3 H_2O	4	0	1.39	1.00
5 H_2O	4	0	1.30	0.96
7.5 H_2O	2	0	*b*	*b*
10 H_2O	2	0	0.20	1.20

[a]Crystallization time t_f, induction time t_0, and kinetics parameters (n_{SH} and k_{SH}) obtained by the SH method with the AE equation of the UiO-66(Zr) solid synthesized at 423 K using $ZrCl_4$ and from 1 to 10 equiv of HCl or H_2O/Zr. Values based on the integration of the (111) Bragg peak. [b]inaccurate fit of n_{SH} and k_{SH} values

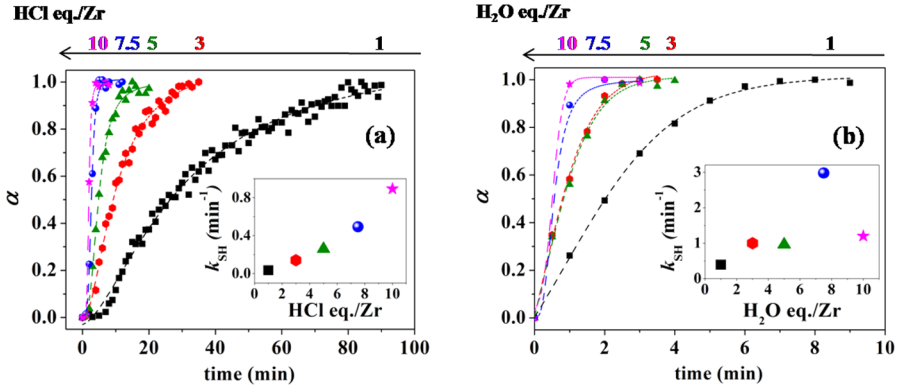

Figure 2. Plots of extent of crystallization α against time, obtained by integration of the (111) Bragg peak of the UiO-66(Zr) solid synthesized at 423 K using $ZrCl_4$ in presence of (a) 1 to 10 equiv of HCl/Zr and (b) 1 to 10 equiv of H_2O/Zr. Crystallization curves were fitted with sigmoidal functions just to direct the eyes. The inset plot shows the crystallization rate k_{SH} as a function of the amount of HCl or H_2O.

dx.doi.org/10.1021/ic402514n | Inorg. Chem. 2014, 53, 2491−2500

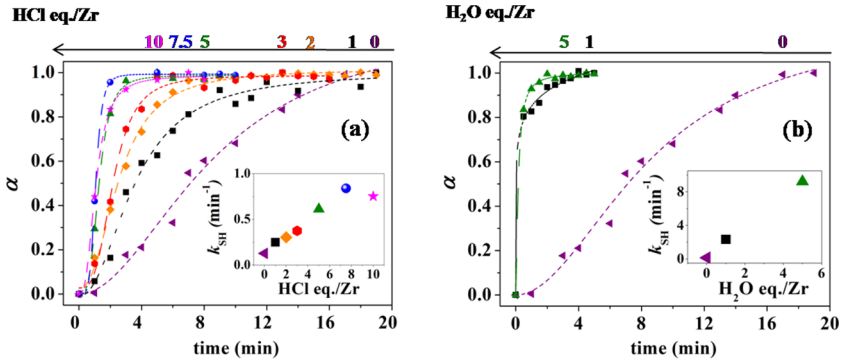

Figure 3. Plots of extent of crystallization α against time, obtained by integration of the (111) Bragg peak of the UiO-66(Zr) solid synthesized at 423 K, using $ZrOCl_2{\cdot}8H_2O$ in presence of (a) 0 to 10 equiv of HCl/Zr and (b) 0 to 10 equiv of H_2O/Zr. Note that the data 0 equiv of HCl and 0 equiv of H_2O correspond to the same data in pure DMF. The inset plot shows the crystallization rate k_{SH} as a function of the HCl or H_2O amount. Note here that eight water molecules are issued from the metallic precursor.

(ranging from 0.2 to 1.9; see Table 1) is consistent with diffusion-limited rate reactions, in which the crystallization rate mainly depends on the diffusion of the reactive species. Remarkably, in the case of low addition of water (1, 3, and 5 equiv of H_2O/Zr), the n_{SH} values are almost constant (1.3 or 1.4) and independent of the water content, suggesting that the same mechanism occurs independently of the H_2O/Zr ratio. This value of $n_{SH} \approx 1.4$ agrees with an instantaneous nucleation,[66] which is consistent with the fast and close crystallization rates obtained for each ratio of H_2O/Zr.

On the contrary, the n_{SH} values seem to increase with the HCl/Zr ratio (n_{SH} (HCl/Zr = 1, 3, and 5) $\approx$ 1.0; n_{SH} (HCl/Zr = 7.5) $\approx$ 1.9, and n_{SH} (HCl/Zr = 10) $\approx$ 1.5), suggesting two different reaction scenarios: (i) at lower HCl/Zr ratios (1, 3, and 5) with slower kinetics and (ii) at higher HCl contents (HCl/Zr = 7.5 and 10) associated with very fast kinetics and instantaneous nucleation. As mentioned above, this is in agreement with the lower acidic conditions that favor the formation of the Zr^{4+} oxo/hydroxo clusters and/or higher HCl/Zr ratio that leads to higher concentration of water.

In light of these data, well-crystalline UiO-66(Zr) solid can be easily prepared over a very short period, that is, within minutes, at ambient pressure from $ZrCl_4$ with the addition of 7.5 equiv of HCl/Zr or 1 equiv of H_2O/Zr (Supporting Information, Figure S31). However, one important drawback of $ZrCl_4$ is its high corrosive and hygroscopic behavior, which may prevent its use for large-scale processes. Indeed the safety data sheet (SDS) of $ZrCl_4$ indicates that it can react violently with water.[67] In addition, $ZrCl_4$ when exposed to air moisture might lead to mixtures of unknown proportions of $ZrCl_4$ and $ZrOCl_2{\cdot}8H_2O$, leading to a difficult handling and reproducibility issues. To avoid these drawbacks, UiO-66(Zr) synthesis was tried using different zirconium precursors such as $ZrOCl_2{\cdot}8H_2O$, ($Zr[acac]_4$), $Zr(SO_4)_2{\cdot}xH_2O$, $(CH_3CO_2)_xZr(OH)_y$ ($x + y = 4$), $Zr(OH)_2CO_3ZrO_2$, and $Zr(O\text{-}^iPr)_4{}^iPrOH$. Only the use of $ZrOCl_2{\cdot}8H_2O$ led to pure UiO-66(Zr) solid, after 24 h at 423 K in the presence of or without HCl (metal/linker/DMF/HCl molar ratio = 1:1:65:0 or 1:1:65:2, note the presence of eight water molecules per Zr in this precursor).

Starting from $ZrOCl_2{\cdot}8H_2O$, the influence of the addition of HCl and H_2O was also evaluated and compared with previous results obtained with the $ZrCl_4$ precursor. The crystallization curves are disclosed in Figure 3 and Supporting Information, Figure S4, and the kinetic information was again extracted and analyzed by the SH method[64] (Table 2 and Supporting Information, Table S5). The synthesis of UiO-66(Zr) solid from $ZrOCl_2{\cdot}8H_2O$ appears less sensitive to additives than the one involving $ZrCl_4$. Here, the addition of neither HCl nor water is needed to form the UiO-66(Zr) solid in pure DMF, while the phase can be obtained in less than 20 min. One has however to consider that eight H_2O/Zr are incorporated when using $ZrOCl_2{\cdot}8H_2O$, which certainly boosts the UiO-66(Zr) solid formation. The comparison of the crystallization curves (see Supporting Information, Figure S6) shows that the synthesis from $ZrCl_4$ with 7.5 equiv of H_2O/Zr presents a faster crystallization than the one from $ZrOCl_2{\cdot}8H_2O$ without addition of H_2O: t_f is 8 times lower (2 vs 16 min) and k_{SH} is more than 20 times higher (2.979 vs 0.128 min^{-1}). However, this could be related to the hygroscopic character of $ZrCl_4$, which might be associated with a slightly hydrated product. Considering a higher water content on the $ZrCl_4$ precursor (Supporting Information, Figure S6), $ZrCl_4$ + 7.5 equiv of H_2O exhibits a kinetics closer to the one of $ZrOCl_2{\cdot}8H_2O$ + 5 H_2O (total H_2O molecules = 13) than the one of $ZrOCl_2{\cdot}8H_2O$. In addition to the confirmation of the hygroscopic character of $ZrCl_4$, this suggests that parameters other than the water content are involved in the difference of formation kinetics of UiO-66(Zr) from $ZrCl_4$ and $ZrOCl_2{\cdot}8$ H_2O precursors. Interestingly, although the reaction is slower when no extra water is added (k_{SH} = 0.128 min^{-1}; see Table 2), no difference could be detected for all experiments with H_2O/Zr > 0 (k_{SH} =

Table 2. [a]

additive (equiv/Zr)	t_f (min)	t_0 (min)	n_{SH}	k_{SH} (min^{-1})
pure DMF	16	1	1.36	0.128
1 HCl	16	1	1.02	0.250
2 HCl	10	0	1.43	0.304
3 HCl	6	0	1.98	0.375
5 HCl	3	0	2.07	0.612
7.5HCl	3	0	0.90	0.839
10 HCl	3	0	0.85	0.752
pure DMF	16	1	1.36	0.128
1 H_2O	4	0	0.38	5.783
5 H_2O	4	0	0.55	5.830

[a]Crystallization time t_f, induction time t_0, and kinetics parameters (n_{SH} and k_{SH}) obtained by the SH method with the AE equation of the UiO-66(Zr) phase at 423 K, using $ZrOCl_2{\cdot}8H_2O$ with addition of 1 to 10 equiv of HCl or H_2O. Values based on the integration of the (111) Bragg peak. Note here that eight water molecules are issued from the metallic precursor.

dx.doi.org/10.1021/ic402514n | Inorg. Chem. 2014, 53, 2491−2500

5.8 min^{-1}; see Table 2). In agreement with what was observed with $ZrCl_4$, the crystallization rate of the UiO-66(Zr) solid in the presence of HCl increases with the amount of HCl, leading to faster crystallization rates (k_{SH} = 0.128 and 0.250 min^{-1} for, respectively, 0 and 1 HCl/Zr).

However, the impact of HCl is much less important than that observed with $ZrCl_4$, as complete crystallization occurred in less than 20 min whatever the amount of HCl added. Although the fitting of the (200) Bragg reflection is less accurate due to its lower signal-to-noise ratio, it is in agreement with our previous results deduced from (111) peak (Supporting Information, Figure S4 and Table S5).

The Avrami exponent coefficients n_{SH} exhibit once more low values (from 0.4 to 2.1; see Table 2), indicating diffusion-limited rate reactions.[66] Similar to previous reactions using $ZrCl_4$, the reaction mechanism seems to be independent of addition of water, with very similar values of n_{SH} (n_{SH} (H_2O/Zr = 1 and 5) ≈ 0.5). Concerning HCl, as observed with $ZrCl_4$, the n_{SH} values increase from 1 to 2 with the HCl content up to HCl/Zr = 5 and then decrease down to 1.

As a summary, three conclusions can be addressed:

(i) the addition of water induces a faster crystallization rate of UiO-66(Zr) solid, favoring the formation of the UiO-66(Zr) oxocluster ($Zr_6(\mu_3\text{-}O)_4(\mu_3\text{-}OH)_4(CO_2)_{12}$). These findings are in agreement with those previously reported by Behrens et al.[48]

(ii) HCl leads to faster crystallization rates of UiO-66(Zr) solid, in agreement with that observed by Katz et al.,[51] but to a lesser extent than the addition of water. As stronger acidic conditions promote the protonation of the linker (pka ≈ 4), slowing down the crystallization rate,[57] the overall faster kinetics is finally attributed to the presence of water from the aqueous HCl solution (12 M).

(iii) Under similar conditions, $ZrCl_4$ (7.5 equiv of H_2O/Zr) speeds up the crystallization of the UiO-66(Zr) solid in comparison with $ZrOCl_2{\cdot}8H_2O$ (Supporting Information, Figure S6).

To shed further light on the crystallization process, temperature-dependent experiments were also carried out at different temperatures (from 343 to 423 K), using both zirconium precursors ($ZrCl_4$ and $ZrOCl_2{\cdot}8H_2O$) and two HCl/Zr ratios (2 and 7.5). Figure 4 and Supporting Information, Figure S5 show the corresponding crystallization curves and SH analyses using the AE nucleation-growth crystallization model (eqs 1 and 2), while Table 3 and Supporting Information, Table S6 give the values of t_f, t_0, n_{SH}, and k_{SH}. Finally, for each precursor and HCl/Zr ratio, pre-exponential factors (A) and activation energies (E_a) were extracted using the Arrhenius equation (eq 3).

$$k = A \exp(-E_a/RT) \quad (3)$$

where k is the rate constant of the chemical reaction at temperature T and R is the universal gas constant.

From these experiments, it seems first that UiO-66(Zr) solid can be prepared over a broad temperature range, the temperature having a very limited effect on the final crystallinity. Furthermore, no crystalline intermediate phase has been observed. Second, as expected, higher temperatures lead to faster crystallization rates (Figure 4a,b,c and Supporting Information, Figure S5a,b,c). More precisely, both crystallization and induction times, disclosed in Table 3, seem to decrease

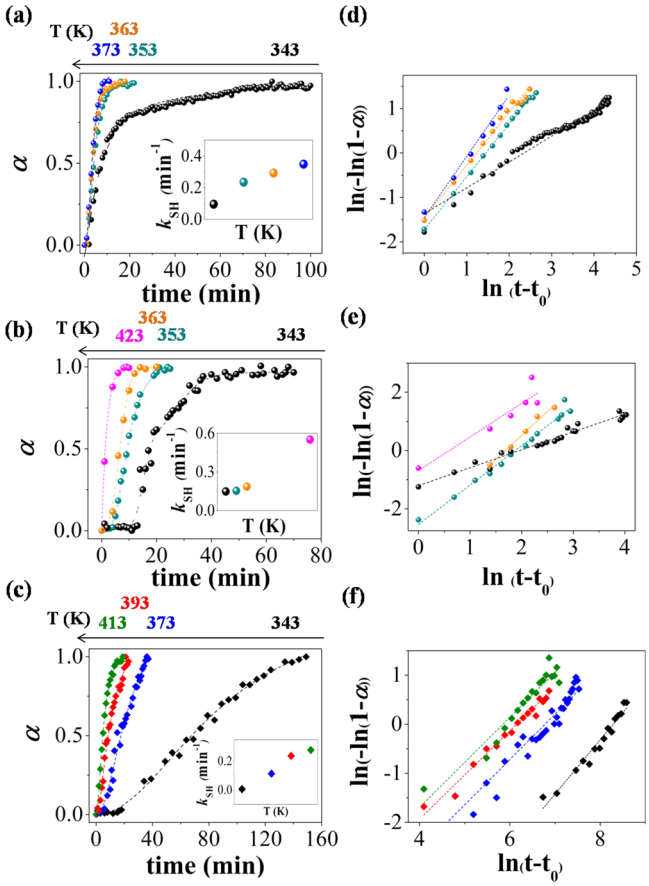

Figure 4. Plots of extent of crystallization α against time obtained by integration of the (111) Bragg peak of the UiO-66(Zr) solid synthesized at four different temperatures and the corresponding SH analyses using the AE nucleation-growth crystallization model: (a) and (d) from 343 to 423 K, using $ZrCl_4$ with 7.5 equiv of HCl/Zr; (b) and (e) from 343 to 423 K, using $ZrOCl_2{\cdot}8H_2O$ with 7.5 equiv of HCl/Zr; (c) and (f) from 343 to 413 K, using $ZrOCl_2{\cdot}8H_2O$ with 2 equiv of HCl/Zr.

following an exponential decay function (Supporting Information, Figure S7). Finally, whatever the temperature, addition of HCl or H_2O still leads to a faster crystallization.

However, the values of the Avrami exponents n_{SH} at 343 K of UiO-66(Zr) syntheses, using 7.5 equiv of HCl/Zr with either $ZrCl_4$ or $ZrOCl_2{\cdot}8H_2O$, are around half of the n_{SH} for the higher temperatures, suggesting a different crystallization mechanism at lower temperatures (see SH plots in Figure 4d,e,f).

Nevertheless, the model of AE has two main drawbacks, as pointed out by Finney et al.:[68] first, the model was initially not adapted for heterogeneous crystallization, and second, nucleation and growth are not considered as separate processes. In contrast, the Gualtieri model[69] considers nucleation and growth as distinct processes, as can be seen in eq 4, where a and b are constants related to the nucleation and k_g and n are, respectively, the rate constant of the crystal growth and the dimension of the growth. Here, we set n = 3 as the UiO-66(Zr) solid crystallizes under a cubic symmetry. The rate constant of nucleation k_n is then calculated by eq 5.

$$\alpha = [1/(1 + \exp -(t - a)/b)][1 - \exp(-k_g t)^n] \quad (4)$$

$$k_n = 1/a \quad (5)$$

dx.doi.org/10.1021/ic402514n | Inorg. Chem. 2014, 53, 2491−2500

Table 3. [a]

T (K)	t_f (min)	t_0 (min)	n_{SH}	k_{SH} (min^{-1})	A (min^{-1})	E_a (kJ mol^{-1})
			$ZrCl_4$ with 7.5 equiv of HCl/Zr			
343	80	2	0.58	0.096	376	22(1)
353	16	1	1.18	0.235		
363	13	1	1.18	0.292		
373	9	1	1.38	0.349		
			$ZrOCl_2{\cdot}8H_2O$ with 7.5 equiv of HCl/Zr			
343	45	14	0.61	0.141	363	22.8(4)
353	21	4	1.35	0.154		
363	14	2	1.64	0.186		
423	8	0	1.15	0.552		
			$ZrOCl_2{\cdot}8H_2O$ with 2 equiv of HCl/Zr			
343	149	20	1.17	0.006	1×10^8	66(16)
373	38	7	0.92	0.114		
393	20	3	0.90	0.237		
413	8	0	0.92	0.278		

[a]Crystallization time t_f, induction time t_0, and kinetics parameters (n_{SH} and k_{SH}) obtained by the SH method with the AE equation as well as calculated pre-exponential factors (A) and activation energies (E_a).

Table 4. [a]

T (K)	a (min)	b (min)	k_g (min^{-1})	k_n (min^{-1})	A_g	$E_{a,g}$ (kJ mol^{-1})	A_n	$E_{a,n}$ (kJ mol^{-1})
				$ZrCl_4$ with 7.5 equiv of HCl/Zr				
343					283	19(6)	12	11(5)
353	4.13(9)	2.35(9)	0.44(2)	0.241(6)				
363	3.47(9)	1.80(9)	0.49(3)	0.287(8)				
373	3.35(5)	1.36(5)	0.63(4)	0.297(4)				
				$ZrOCl_2{\cdot}8H_2O$ with 7.5 equiv of HCl/Zr				
343	15(4)	9(2)	0.064(9)	0.07	9547	31(12)	8782	32(13)
353	9.1(2)	3.1(2)	0.17(1)	0.1(0)				
363	3.1(1)	0.83(7)	0.47(7)	0.3(0)				
423	1.1(2)	1.4(1)	1.2(1)	0.9(1)				
				$ZrOCl_2{\cdot}8H_2O$ with 2 equiv of HCl/Zr				
343	71.1(6)	27.4(7)	0.039(4)	0.0141(2)	1×10^5	46(2)	2×10^4	39(1)
373	19.2 (4)	8.3 (5)	0.11(1)	0.052(1)				
393	8.2(4)	5.3(4)	0.21(2)	0.121(6)				
413	4.7(3)	3.6(3)	0.38(4)	0.21(1)				

[a]Kinetics parameters (a, b, k_g, and k_n) obtained by the Gualtieri equation as well as calculated pre-exponential factors (A_g and A_n) and activation energies ($E_{a,g}$ and $E_{a,n}$) for both nucleation and growth.

Millange et al.[54] have validated this model for the crystallization of the MOF-14 and HKUST-1. Consequently, this second model was used here, disclosing the values of a, b, k_g, and k_n in Table 4 and Supporting Information, Table S7. Pre-exponential factors corresponding to nucleation (A_n) and growth processes (A_g) as well as activation energies of nucleation ($E_{a,n}$) and growth regions ($E_{a,g}$) were also estimated (Table 4 and Supporting Information, Table S7).

k_g is higher than k_n, indicating that the nucleation process is rate-limiting. In addition, the activation energies of the nucleation and the growth are not significantly different (Table 4), being in agreement with those extracted from the AE model ($E_{a,n} \approx E_{a,g}$ = 19(6), 31(12), and 46(2) vs E_a = 22(1), 22.8(4), and 66(16) kJ mol^{-1} for, respectively, $ZrCl_4$ with 7.5 equiv of HCl/Zr, $ZrOCl_2{\cdot}8H_2O$ with 7.5 equiv of HCl/Zr, and $ZrOCl_2{\cdot}8H_2O$ with 2 equiv of HCl/Zr). Considering the short induction time, similar activation energies for nucleation and crystal growth were expected, as already observed by Cravillon et al.[57] Nevertheless, a small difference between $E_{a,n}$ and $E_{a,g}$ can be seen. Similar observations were made in the crystallization of the CPO-27(Co) solid upon the addition of formate,[60] which was assumed to be due to a change in nucleation and growth balance through a chemical interaction with the formate. In our case, the addition of HCl might modify the nucleation and growth balance by accelerating nucleation, which could explain the difference between both energies. In the case of 7.5 equiv of HCl/Zr, the activation energies are very close, suggesting that activation energy seems to be independent of the precursor. However, these activation energy values are less than half of those obtained in the presence of 2 equiv of HCl/Zr (~22 vs 66 kJ mol^{-1}), indicating that the presence of HCl decreases the activation energy. Indeed, in agreement with the aqueous chemistry of zirconium,[65] decreasing the pH of the reaction mixture by adding HCl might lead to an easier stabilization of the Zr^{4+} oxo/hydroxo clusters, which could explain the decrease of the activation energy when more HCl is added.

Finally, the use of $ZrOCl_2{\cdot}8H_2O$ with 2 equiv of HCl/Zr leads to a much higher pre-exponential factor (A) than with $ZrCl_4$ and $ZrOCl_2{\cdot}8H_2O$ with 7.5 equiv of HCl/Zr. This seems at first sight to be in disagreement with what was reported previously. However, Ahnfeldt et al.[56] have attributed this

dx.doi.org/10.1021/ic402514n | Inorg. Chem. 2014, 53, 2491−2500

Table 5. [a]

Zr precursor	(equiv of additive)/Zr	particle size (nm)	PDI[b]	wt % ZrO_2 TGA[c,d]	yield[e] (%)
$ZrCl_4$	1 HCl	940(62)	0.25	50.6	66
	7.5 HCl	575(45)	0.20	42.4	73
	1 H_2O	776(58)	>0.3	51.0	29
	7.5 H_2O	458(91)	>0.3	52.2	46
$ZrOCl_2{\cdot}8H_2O$	1 HCl	299(17)	>0.3	47.9	76
	7.5 HCl	378(107)	>0.3	48.4	78
	1 H_2O	258(22)	>0.3	63.6	56
	7.5 H_2O	409(149)	0.27	52.2	77

[a]Particle size determination by DLS in ethanol, estimated yield based on zirconium and TGA calculations of the UiO-66(Zr) synthesized at 423 K using $ZrCl_4$ and $ZrOCl_2{\cdot}8H_2O$ with the addition of 1 and 7.5 equiv of HCl or H_2O. [b]Polydispersity index. [c]% ZrO_2 (theoretical ZrO_2 percentage for an ideal 12-connected Zr_6 cluster: 45.4 wt %). [d]All data have considered the dry dehydroxylated solid with the formula $Zr_6O_6(BDC)_6$. [e]Details on the yield calculation can be found in the Supporting Information (page S28).

increase of pre-exponential factor to an acceleration of the crystal growth stage in the case of CAU-1(Al)-NH_2.

To select the most promising reaction conditions for the large lab-scale synthesis of UiO-66(Zr), the crystallinity, oxide percentage, and yield were evaluated. Accordingly, for each precursor a low and high ratio of HCl and H_2O/Zr was selected (1 and 7.5 equiv), quenching the reaction at t_f. After filtration and purification with DMF and MeOH, the UiO-66(Zr) samples were fully characterized by dynamic light scattering (DLS), X-ray powder diffraction (XRPD), and thermogravimetric analysis (TGA). All these results can be found in Table 5 and Supporting Information, Figures S31 and S32.

On the whole, the UiO-66(Zr) samples made from $ZrCl_4$ exhibit a narrower full width at half-maximum (FWHM) of the main diffraction peaks (Supporting Information, Figure S31), suggesting a larger crystallite size and/or the presence of fewer defects or stacking faults. Notably, the addition of a small amount of HCl (1 equiv/Zr) seems to improve the FWHM of the UiO-66(Zr) synthesized from $ZrOCl_2{\cdot}8H_2O$ in comparison with the addition of H_2O (1 equiv/Zr). On the other hand, higher amounts of HCl lead to a lower fwhm for both Zr precursors.

In agreement with XRPD, larger particle sizes were observed for $ZrCl_4$, except in presence of large amounts of water, where both precursors led to similar particle (submicrometer) dimensions (Table 5). Note however that considering the eight water molecules of $ZrOCl_2{\cdot}8H_2O$, the crystal size is not significantly different from that of the $ZrCl_4$/7.5 equiv of H_2O (409 ± 149 vs 458 ± 91 nm). Remarkably, the particle size can be easily tuned. While almost micrometric crystals are obtained when using the $ZrCl_4$ precursor and small amounts of HCl or H_2O (940 ± 62 and 776 ± 58 nm, respectively), submicronic particles of ca. 300 nm are formed with $ZrOCl_2{\cdot}8H_2O$ in the presence of a small amount of HCl or H_2O. Furthermore, smaller and rather monodispersed UiO-66(Zr) particles of 100 ± 20 nm can be prepared using $ZrOClO_2{\cdot}8H_2O$, with addition of HCl or H_2O, at short times (2 h). This interesting result paves the way for the use of UiO-66(Zr) within the nanotechnology field (sensors, drug release, films, etc.).[47,48]

The yield of the reaction based on zirconium was evaluated for various precursor/additive couples (Table 5). On the whole, the use of $ZrOCl_2{\cdot}8H_2O$ leads to significantly higher yields compared with $ZrCl_4$. Addition of large amounts of HCl or H_2O also improve the yield, although to a lesser extent. Concerning TGA, it can be concluded that using $ZrOCl_2{\cdot}8H_2O$ as the precursor with the addition of HCl does not lead to the formation of denser inorganic impurities (most probably ZrO_2, as suggested from XRPD) compared to the $ZrCl_4$ route. Remarkably, the presence of linker vacancies in the UiO-66(Zr) structure, which have been pointed out in the literature,[45,70−72] might explain the slight differences between calculated and observed weight loss percentage. Nevertheless, when adding H_2O, particularly in the case of the $ZrOCl_2{\cdot}8H_2O$ precursor, the larger difference cannot be attributed solely to the presence of defects and certainly corresponds to the formation of ZrO_2, which can strongly decrease the final porosity (Table 5 and Supporting Information, Figure S32).

Laboratory Scale-up. From the above-mentioned results, the scaled-up synthesis of UiO-66(Zr) solid was carried out using $ZrOCl_2{\cdot}8H_2O$ and the addition of HCl (Supporting Information, Figure S35). In the first step, a zirconium concentration of 0.2 M was used together with the addition of 2 equiv of HCl/Zr in a 1 L reactor. Twenty-six grams of a pure and well-crystallized UiO-66(Zr) was obtained with a STY of 51 kg m^3 day^{-1} (calculated only in terms of volume of the reaction mixture and reaction time) and a yield of about 80% (Supporting Information, Figure S36 to S39). Nitrogen adsorption isotherms (Supporting Information, Figure S39) confirm the high microporous character of the product, very similar to the reported values (S_{BET} = 1050 m^2 g^{-1} and V_p = 0.47 cm^3 g^{-1}).[33,70] Nevertheless, the characteristic microporous type I isotherm showed an important adsorption above p/p_0 = 0.85, in agreement with the presence of an important degree of interparticular mesoporosity due to the small size of the particles.

The effect of the concentration of the reactants (0.2, 0.4, and 1.0 M) was further examined using first a small volume of solvent (50 mL). Increasing the concentration above 0.2 M led to a fast gelation of the reaction medium, without any effect on the final crystallinity (Supporting Information, Figure S33 and S34) and accessible porosity. Thus, in a final stage, a larger batch of UiO-66(Zr) was produced using a 5 L reactor and a high concentration of reactants (∼1 M). This led to the formation of a white gel even at room temperature, which was further heated above 363 K for 8 h. About 510 g of well-crystallized UiO-66(Zr) was finally obtained, together with a reaction yield of 67% (Supporting Information, Figures S40 and S41). The resulting STY was estimated to 490 kg m^{-3} day^{-1}, a value sufficiently high for mass production, considering those of most commercial Basolites reported by BASF SE.[12,29] Moreover, the final UiO-66(Zr) product after activation exhibited a very high porosity (S_{BET} = 1375 m^2 g^{-1} and Vp = 1.27 cm^3 g^{-1}) (Figure 5).

dx.doi.org/10.1021/ic402514n | Inorg. Chem. 2014, 53, 2491−2500

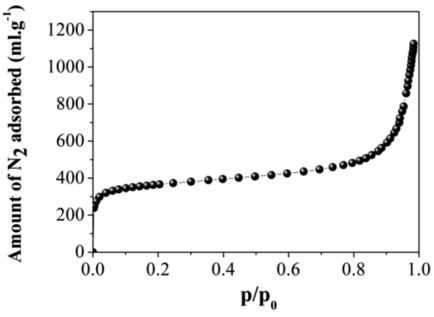

Figure 5. N_2 sorption isotherm at 77 K of the UiO-66(Zr) solid obtained from the scale-up synthesis using a 5 L reactor.

Finally, this strategy was applied to the multigram, atmospheric pressure synthesis of several functionalized derivatives of UiO-66(Zr) based on terephthalate linkers bearing −Br, $-NH_2$, and $-NO_2$ groups.[73] Respectively, 8, 12, and 3 g of pure and well-crystallized UiO-66(Zr)−Br, $-NH_2$, and $-NO_2$ were obtained with STYs of 118, 109, and 250 kg m^{-3} day^{-1} and yields of 92, 73, and 58%, respectively.

CONCLUSION

The main parameters affecting the kinetics of crystallization of the archetypical microporous UiO-66(Zr) were evaluated using time-resolved in situ EDXRD. The addition of hydrochloric acid and water led to faster crystallization, together with a decrease of the activation energy of the reaction. Moreover, reproducibility and safety issues related to the $ZrCl_4$ precursor could be avoided by using $ZrOCl_2{\cdot}8H_2O$, which also led to significantly higher reaction yields. Furthermore, this allowed the reduction of the particle size to a few hundred nanometers without affecting the physicochemical properties, paving the way for further use within the nanotechnology field.

Finally, the preparation of UiO-66(Zr) at ambient pressure was scaled up from a 20 g scale (laboratory) to the 500 g scale (pilot) with rather high STY. In both cases, the final products exhibited physicochemical properties comparable to those observed from smaller batches.

ASSOCIATED CONTENT

Supporting Information

Tables listing UiO-66(Zr) synthesis conditions for in situ crystallization studies, representation of the UiO-66(Zr) structure, crystallization curves of the UiO-66(Zr) (200) Bragg peak, Sharp-Hancock plots, nonlinear Gualtieri fits, and Arrhenius plots as well as characterizations of the UiO-66(Zr) samples prepared at the laboratory scale. This material is available free of charge via the Internet at http://pubs.acs.org.

AUTHOR INFORMATION

Corresponding Authors

*E-mail: patricia.horcajada-cortes@uvsq.fr (P.H.).
*E-mail: christian.serre@uvsq.fr (C.S.).

Present Addresses

∥(F.R.) School of Chemistry, The University of Sydney, Sydney, New South Wales 2006, Australia
⊥(H.C.) Australian Nuclear Science and Technology Organisation (ANSTO), Bragg Institute, Menai, New South Wales 2234, Australia.
⊗(S.R.M.) UOP Research Center, UOP LLC, a Honeywell Compagny, 25 East Algonquin Road, Des Plaines, Illinois 60017, United States.

Notes

The authors declare no competing financial interest.

ACKNOWLEDGMENTS

The research leading to these results has received funding from the European Community's Seventh Framework Program (FP7/2007-2013) under Grant Agreement No. 228862. Korean authors are grateful to the Korea CCS R&D Center (KCRC) for financial support (NRF-2011-0031982) and to the ISTK for the interinstitutional collaboration program (SK-1210). We thank DESY synchrotron facilities for award of beamtime at F3 beamline HASYLAB, Dr. A. Rothkirch (DESY) for the software support, the Christian-Albrechts-Universität team of Prof. W. Bensch (Kiel, Germany) for lending us the in situ furnace device, and the group of Prof. N. Stock, especially M. Feyand, for their helpful assistance using the beamline.

REFERENCES

(1) Eddaoudi, M.; Moler, D. B.; Li, H.; Chen, B.; Reineke, T. M.; O'Keeffe, M.; Yaghi, O. M. *Acc. Chem. Res.* **2001**, *34*, 319−330.
(2) See MOFs special issue: *Chem. Rev.* **2012**, *112*, 673-1268.
(3) See MOFs special issue: *Microporous Mesoporous Mater.***2012**, *157*, 1-145.
(4) Dincă, M.; Long, J. R. *Angew. Chem., Int. Ed.* **2008**, *47*, 6766−6779.
(5) Murray, L. J.; Dincă, M.; Long, J. R. *Chem. Soc. Rev.* **2009**, *38*, 1294−1314.
(6) Li, J.-R.; Ma, Y.; McCarthy, M. C.; Sculley, J.; Yu, J.; Jeong, H.-K.; Balbuena, P. B.; Zhou, H.-C. *Coord. Chem. Rev.* **2011**, *255*, 1791−1823.
(7) Suh, M. P.; Park, H. J.; Prasad, T. K.; Lim, D.-W. *Chem. Rev.* **2012**, *112*, 782−835.
(8) Farrusseng, D.; Aguado, S.; Pinel, C. *Angew. Chem., Int. Ed.* **2009**, *48*, 7502−7513.
(9) Dhakshinamoorthy, A.; Garcia, H. *Chem. Soc. Rev.* **2012**, *41*, 5262−5284.
(10) Horcajada, P.; Chalati, T.; Serre, C.; Gillet, B.; Sebrie, C.; Baati, T.; Eubank, J. F.; Heurtaux, D.; Clayette, P.; Kreuz, C.; Chang, J.-S.; Hwang, Y. K.; Marsaud, V.; Bories, P.-N.; Cynober, L.; Gil, S.; Férey, G.; Couvreur, P.; Gref, R. *Nat. Mater.* **2010**, *9*, 172−178.
(11) Della Rocca, J.; Liu, D.; Lin, W. *Acc. Chem. Res.* **2011**, *44*, 957−968.
(12) Czaja, A. U.; Trukhan, N.; Mueller, U. *Chem. Soc. Rev.* **2009**, *38*, 1284−1293.
(13) Gaab, M.; Trukhan, N.; Maurer, S.; Gummaraju, R.; Mueller, U. *Microporous Mesoporous Mater.* **2012**, *157*, 131−136.
(14) Yilmaz, B.; Trukhan, N.; Mueller, U. *Chin. J. Catal.* **2012**, *33*, 3−10.
(15) Mueller, U.; Puetter, H.; Hesse, M.; Wessel, H. Patent WO 2005/049892, 2005.
(16) Mueller, U.; Richter, I.; Schubert, M. Patent WO 2007/131955 A1, 2007.
(17) Jhung, S. H.; Chang, J.-S. Patents KR 0627634; JP 4610531, 2007.
(18) Schubert, M.; Mueller, U.; Mattenheimer, H.; Tonigold, M. Patent WO 2007/023119, 2007.
(19) Schubert, M.; Mueller, U.; Tonigold, M.; Ruetz, R. Patent WO 2007/023134 A1, 2007.
(20) Chang, J.-S.; Hwang, Y. K.; Jhung, S. H. Patent WO 2008/066293 A1, 2008.
(21) Chang, J.-S.; Hwang, Y. K.; Jhung, S. H.; Hwang, J.-S.; Seo, Y.-K. Patent KR 0803945, 2008.
(22) Leung, E.; Mueller, U.; Cox, G. Patent WO 2010/106121 A1, 2010.

(23) Leung, E.; Mueller, U.; Cox, G.; Mattenheimer, H.; Trukhan, N.; Blei, S. EP Patent registration 10183283.0, in press.
(24) Schubert, M.; Mueller, U.; Marx, S. Patent WO 2008/129051, 2008.
(25) Mueller, U.; Schubert, M.; Teich, F.; Puetter, H.; Schierle-Arndt, K.; Pastré, J. *J. Mater. Chem.* **2006**, *16*, 626−636.
(26) Sigma-Aldrich Home Page. http://www.sigmaaldrich.com (accessed December 16, 2013).
(27) Gritzner, G.; Kreysa, G. *Pure Appl. Chem.* **1993**, *65*, 1009−1020.
(28) Seo, Y.-K.; Yoon, J. W.; Lee, J. S.; Lee, U. H.; Hwang, Y. K.; Jun, C.-H.; Horcajada, P.; Serre, C.; Chang, J.-S. *Microporous Mesoporous Mater.* **2012**, *157*, 137−145.
(29) Stock, N.; Biswas, S. *Chem. Rev.* **2012**, *112*, 933−969.
(30) Cbana Labs, Inc Home Page. http://cbana.com (accessed December 16, 2013).
(31) Wu, T.; Shen, L.; Luebbers, M.; Hu, C.; Chen, Q.; Ni, Z.; Masel, R. I. *Chem. Commun.* **2010**, *46*, 6120−6122.
(32) Low, J. J.; Benin, A. I.; Jakubczak, P.; Abrahamian, J. F.; Faheem, S. A.; Willis, R. R. *J. Am. Chem. Soc.* **2009**, *131*, 15834−15842.
(33) Cavka, J. H.; Jakobsen, S.; Olsbye, U.; Guillou, N.; Lamberti, C.; Bordiga, S.; Lillerud, K. P. *J. Am. Chem. Soc.* **2008**, *130*, 13850−13851.
(34) Wiersum, A. D.; Soubeyrand-Lenoir, E.; Yang, Q.; Moulin, B.; Guillerm, V.; Yahia, M. B.; Bourelly, S.; Vimont, A.; Miller, S.; Vagner, C.; Daturi, M.; Clet, G.; Serre, C.; Maurin, G.; Llewellyn, P. L. *Chem.—Asian J.* **2011**, *6*, 3270−3280.
(35) Kim, M.; Cohen, S. M. *CrystEngComm* **2012**, *14*, 4096−4104.
(36) Garibay, S. J.; Cohen, S. M. *Chem. Commun.* **2010**, *46*, 7700−7702.
(37) Kandiah, M.; Nilsen, M. H.; Usseglio, S.; Jakobsen, S. r.; Olsbye, U.; Tilset, M.; Larabi, C.; Quadrelli, E. A.; Bonino, F.; Lillerud, K. P. *Chem. Mater.* **2010**, *22*, 6632−6640.
(38) Guillerm, V.; Ragon, F.; Dan-Hardi, M.; Devic, T.; Vishnuvarthan, M.; Campo, B.; Vimont, A.; Clet, G.; Yang, Q.; Maurin, G.; Férey, G.; Vittadini, A.; Gross, S.; Serre, C. *Angew. Chem., Int. Ed.* **2012**, *51*, 9267−9271.
(39) Yang, Q.; Wiersum, A. D.; Jobic, H.; Guillerm, V.; Serre, C.; Llewellyn, P. L.; Maurin, G. *J. Phys. Chem. C* **2011**, *115*, 13768−13774.
(40) Yang, Q.; Wiersum, A. D.; Llewellyn, P. L.; Guillerm, V.; Serre, C.; Maurin, G. *Chem. Commun.* **2011**, *47*, 9603−9605.
(41) Yang, Q.; Jobic, H.; Salles, F.; Kolokolov, D.; Guillerm, V.; Serre, C.; Maurin, G. *Chem.—Eur. J.* **2011**, *17*, 8882−8889.
(42) Barcia, P. S.; Guimarães, D.; Mendes, P. A. P.; Silva, J. A. C.; Guillerm, V.; Chevreau, H.; Serre, C.; Rodrigues, A. E. *Microporous Mesoporous Mater.* **2011**, *139*, 67−73.
(43) Silva, C. G.; Luz, I.; Llabrés i Xamena, F. X.; Corma, A.; García, H. *Chem.—Eur. J.* **2010**, *16*, 11133−11138.
(44) Vermoortele, F.; Ameloot, R.; Vimont, A.; Serre, C.; De Vos, D. *Chem. Commun.* **2011**, *47*, 1521−1523.
(45) Vermoortele, F.; Bueken, B.; Le Bars, G.; Van de Voorde, Ben.; Vandichel, M.; Houthoofd, K.; Vimont, A.; Daturi, M.; Waroquier, M.; Van Speybrieck, V.; Kirschhock, C.; De Vos, D. E. *J. Am. Chem. Soc.* **2013**, *135*, 11465−11468.
(46) Cunha, D.; Gaudin, C.; Colinet, I.; Horcajada, P.; Maurin, G.; Serre, C. *J. Mater. Chem. B* **2013**, *1*, 1101−1108.
(47) Abid, H. R.; Ang, H. M.; Wang, S. *Nanoscale* **2012**, *4*, 3089−3094.
(48) Schaate, A.; Roy, P.; Godt, A.; Lippke, J.; Waltz, F.; Wiebcke, M.; Behrens, P. *Chem.—Eur. J.* **2011**, *17*, 6643−6651.
(49) Wibmann, G.; Schaate, A.; Lilienthal, S.; Bremer, I.; Schneider, A. M.; Behrens, P. *Microporous Mesoporous Mater.* **2012**, *152*, 64−70.
(50) Zlotea, C.; Phanon, D.; Mazaj, M.; Heurtaux, D.; Guillerm, V.; Serre, C.; Horcajada, P.; Devic, T.; Magnier, E.; Cuevas, F.; Férey, G.; Llewellyn, P. L.; Latroche, M. *Dalton Trans.* **2011**, *40*, 4879−4881.
(51) Katz, M. J.; Brown, Z. J.; Colón, Y. J.; Siu, P. W.; Scheidt, K. A.; Snurr, R. Q.; Hupp, J. T. Hupp; Farha, O. M. *Chem. Commun.* **2013**, *49*, 9449−9451.
(52) Schoenecker, P. M.; Belancik, G. A.; Grabicka, B. E.; Walton, K. S. *AIChE J.* **2013**, *59*, 1255−1262.
(53) Millange, F.; Medina, M.; Guillou, N.; Férey, G.; Golden, K.; Walton, R. *Angew. Chem., Int. Ed.* **2010**, *49*, 763−766.
(54) Millange, F.; El Osta, R.; Medina, M. E.; Walton, R. I. *CrystEngComm* **2011**, *13*, 103−108.
(55) Ahnfeldt, T.; Moellmer, J.; Guillerm, V.; Staudt, R.; Serre, C.; Stock, N. *Chem.—Eur. J.* **2011**, *17*, 6462−6468.
(56) Ahnfeldt, T.; Stock, N. *CrystEngComm* **2012**, *14*, 505−511.
(57) Cravillon, J.; Schroder, C. A.; Bux, H.; Rothkirch, A.; Caro, J.; Wiebcke, M. *CrystEngComm* **2012**, *14*, 492−498.
(58) El Osta, R.; Frigoli, M.; Marrot, J.; Medina, M. E.; Walton, R. I.; Millange, F. *Cryst. Growth Des.* **2012**, *12*, 1531−1537.
(59) Reinsch, H.; Stock, N. *CrystEngComm* **2013**, *15*, 544−550.
(60) El Osta, R.; Feyand, M.; Stock, N.; Millange, F.; Walton, R. I. *Powder Diffr.* **2013**, *28*, S256−S275.
(61) Engelke, L.; Schaefer, M.; Schur, M.; Bensch, W. *Chem. Mater.* **2001**, *13*, 1383−1390.
(62) Avrami, M. *J. Chem. Phys.* **1941**, *9*, 177−184.
(63) Erofe'ev, B. V. *C. R. (Dokl.) Acad. Sci. URSS* **1946**, *52*, 511−514.
(64) Sharp, J. D.; Hancock, J. H. *J. Am. Ceram. Soc.* **1972**, *55*, 74−77.
(65) Kaye, M. H.; Thompson, W. T. Chapter 9. In *Uhlig's Corrosion Handbook*, 3rd ed.; John Wiley & Sons: Hoboken, NJ, 2011.
(66) Hulbert, S. F. *J. Br. Ceram. Soc.* **1969**, *6*, 11.
(67) Downloadable free of charge in the Sigma-Aldrich web site: http://www.sigmaaldrich.com/safety-center.html (accessed December 16, 2013).
(68) Finney, E. E.; Finke, R. G. *Chem. Mater.* **2009**, *21*, 4692−4705.
(69) Gualtieri, A. F. *Phys. Chem. Miner.* **2001**, *28*, 719−728.
(70) Valenzano, L.; Civalleri, B.; Chavan, S.; Bordiga, S.; Nilsen, M. H.; Jakobsen, S. R.; Lillerud, K. P.; Lamberti, C. *Chem. Mater.* **2011**, *23*, 1700−1718.
(71) Wu, H.; Chua, Y. S.; Krungleviciute, V.; Tyagi, M.; Chen, P.; Yildirim, T.; Zhou, W. *J. Am. Chem. Soc.* **2013**, *135*, 10525−10532.
(72) Xydias, P.; Spanopoulos, I.; Klontzas, E.; Froudakis, G. E.; Trikalitis, P. N. *Inorg. Chem.* [Online early access]. DOI: 10.1021/ic402430n.
(73) Mendes, P. A. P.; Ragon, F.; Rodrigues, A. E.; Horcajada, P.; Serre, C.; Silva, J. A. C. *Microporous Mesoporous Mater.* **2013**, *170*, 251−258.